



**HAL**  
open science

## Developing a GIS Tool for Emergency Urban Cooling in Case of Heat-Waves

Martin Hendel, Cécilia Bobée, Ghid Karam, Sophie Parison, Alexandre Berthe, Patricia Bordin

### ► To cite this version:

Martin Hendel, Cécilia Bobée, Ghid Karam, Sophie Parison, Alexandre Berthe, et al.. Developing a GIS Tool for Emergency Urban Cooling in Case of Heat-Waves. *Urban Climate*, 2020, 33, pp.100646. 10.1016/j.uclim.2020.100646 . hal-02473067

**HAL Id: hal-02473067**

**<https://hal.science/hal-02473067>**

Submitted on 10 Feb 2020

**HAL** is a multi-disciplinary open access archive for the deposit and dissemination of scientific research documents, whether they are published or not. The documents may come from teaching and research institutions in France or abroad, or from public or private research centers.

L'archive ouverte pluridisciplinaire **HAL**, est destinée au dépôt et à la diffusion de documents scientifiques de niveau recherche, publiés ou non, émanant des établissements d'enseignement et de recherche français ou étrangers, des laboratoires publics ou privés.

# Developing a GIS Tool for Emergency Urban Cooling in Case of Heat-Waves

Martin Hendel<sup>1,2</sup>, Cécilia Bobée<sup>1</sup>, Ghid Karam<sup>1,2</sup>, Sophie Parison<sup>1,3</sup>, Alexandre Berthe<sup>1,4</sup>, Patricia Bordin<sup>1,5</sup>

<sup>1</sup> Université de Paris, LIED, UMR 8236, CNRS, F-75013, Paris, France

<sup>2</sup> Université Gustave Eiffel, ESIEE Paris, département SEN, F-93162, Noisy-le-Grand, France

<sup>3</sup> Paris City Hall, Paris, France

<sup>4</sup> Univ Rennes, LiRIS, EA 7481, F-35000, Rennes, France.

<sup>5</sup> Université Paris-Est, ESTP, Institut de Recherche en Constructibilité, F-94234, Cachan, France

## Abstract

Many cities are expected to face a strong increase in the frequency and intensity of heat-waves by the end of the 21<sup>st</sup> Century due to climate change. In Paris, the frequency of heat-waves could rise from an average of one day per year to 14-26 days per year, with temperatures reaching up to 50°C. Since 2012, pavement-watering is viewed as a potential tool for emergency cooling by the city while scientific work on the technique has found its application to be best suited to densely built urban areas, compared for example to urban greening whose impact may be hindered by lack of available planting space.

This paper proposes an interdisciplinary approach combining urban physics with social sciences to develop such a GIS model for pavement-watering as an emergency response to heat-waves in Paris. It is built on performance criteria derived from previous work are input into a Geographic Information System to identify urban areas where pavement-watering would be most effective. In addition, a heat-related health risk assessment is conducted, using microclimatic, urban and socio-economic layers, to single out areas where heat-wave risk is highest in public spaces, combining high temperatures, pedestrian traffic and local population vulnerability. The microclimatic hazard dataset includes a physical model of park and water body cool islands assuming they are driven by thermal diffusion.

The resulting tool has significant flexibility in defining the thresholds of the different indicators. The mapping scheme identified a total of 50 to 200 km of high priority areas for pavement-watering, requiring between 1,400 and 5,800 m<sup>3</sup>/day of non-potable water, equivalent to 0.6 to 2.6 L/day per capita. Limitations due to data quality or resolution are discussed as well as paths for further improvement.

## Keywords

Climate change adaptation; heat waves; urban cooling; emergency heat wave response; decision support tool

## Nomenclature

<i>AM</i>	air mass	<i>SA</i>	short axis
DEM	digital elevation model	SW	shortwave
GIS	geographic information system	$R_n$	net radiation
<i>H</i>	atmospheric convection	UTCI	Universal Thermal Climate Index
HVI	heat vulnerability index	<b>Superscripts/subscripts</b>	
<i>I</i>	solar irradiance	ETR	extraterrestrial
<i>L</i>	longwave radiation	G	global horizontal
<i>LA</i>	long axis	ref	reflected
<i>S</i>	shortwave radiation	up	upwards

## Introduction

As a result of climate change, many cities including Paris are expected to face a strong increase in the frequency and intensity of heat-waves by the end of the 21<sup>st</sup> Century, with certain regions facing the risk of

becoming uninhabitable at least part of the year [1]–[3]. In Paris, the frequency of heat-waves could rise from an average of one day per year to 14–26 days per year [4], with temperatures reaching up to 50°C [5]. Since 2012, pavement-watering is viewed as a potential tool for emergency cooling by Paris City Hall with references made in a number of City documents such as the Climate Adaptation Strategy [6], [7]. The method has been thoroughly studied in Japan and France, both with field and lab experiments as well as computer simulations and has been found to be best suited to densely built urban areas where road surfaces are most present and urban greening may be hindered for lack of available space [8]–[13].

Pavement-watering is a technique based on the Japanese practice named “Uchimizu” [14]. It essentially consists in generating a latent heat flow on otherwise dry surfaces, by sprinkling water onto impervious sidewalk and road surfaces for example during heat-waves. Cooling is provided mainly as the sprinkled water evaporates from the ground and marginally as excess water heats up and runs off into the sewer system, as illustrated in Figure 1.

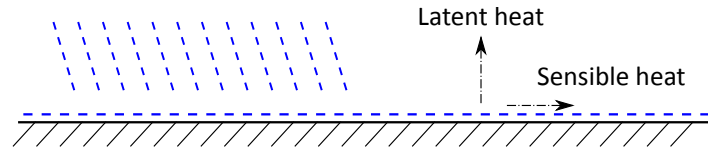


Figure 1: Cooling mechanisms of pavement-watering.

In Paris, the method has been studied in the field every summer since 2012, focusing on its thermal and microclimatic effects as well as its water consumption. This work has found that pavement-watering is responsible for thermal effects such as temperature reductions of 13°C and 5°C on average during insolation at the pavement surface and 5 cm deep, respectively [15], [16]. Furthermore, heat absorption was found to be cut at least in half, i.e. a decrease of up to 150 W/m<sup>2</sup> [17]. In addition, these tests led to the development of field methods for quantifying pavement-watering’s microclimatic impacts [18]. These were found to represent UTCI-equivalent temperature reductions of up to 2.8°C, concurrent with peak outdoor temperatures, as well as small but statistically significant effects on the urban heat island (UHI) [18], [19]. This work is still underway with new field test sites being instrumented and including the use of new pavement structures, parallel to the thermo-climatic characterization of pavement structures in the lab, with and without watering [20], [21].

In essence, studies have found that the following conditions lead to the greatest pavement-watering cooling effects while minimizing water consumption:

- Thermal effects are greatest for an insulated surface
- Microclimatic effects are greatest concurrently with peak daily temperatures
- Microclimatic effects are greatest outdoors, closest to the watered surface
- Only enough water should be sprinkled for evaporation while avoiding any runoff, but without letting the surface dry completely

These criteria are essential when designing a pavement-watering strategy for a given urban area and can be used with corresponding data layers in a Geographic Information System (GIS) to identify urban areas where pavement-watering would be most effective. In addition, an urban heat wave risk map can also be used to focus on areas with the highest heat hazard, greatest population exposure and highest vulnerability.

To date, a number of mapping approaches have been developed with the aim of identifying urban areas with the greatest heat risks [22]–[24]. Many of these approaches use satellite-derived surface temperature measurements as a proxy for daytime air temperatures. However, none of these approaches aims to assist decision-makers in the deployment of an urban cooling strategy.

Many cities in the English-speaking world have used and applied Heat Vulnerability Index (HVI) mapping [25]–[28]. These tools are cited as being useful for the purpose of emergency response to heat-waves or for longer-term planning measures. However, the dominant approach of conflating a large number of indicators modelling different aspects of heat risk has been shown in some instances to be ill-suited to the task of heat mortality prediction and consequently heat risk evaluation [29].

This paper proposes an interdisciplinary approach combining urban physics with social sciences to develop a GIS model to assist urban decision makers prioritize target areas for pavement-watering as an emergency response to heat-waves in Paris. Limitations due to data quality or resolution are discussed as well as paths for further improvement, including discriminating areas according to their pavement type.

# Methodology

## Study objectives and framework

The proposed decision-support GIS tool aims to assist Parisian decision-makers in designing a pavement-watering strategy as an emergency response to heat-waves. The boundaries of the study area are the Paris city limits, also known as “Paris intra-muros”. Because the plan will be deployed by Paris City Hall, the target areas within the city are all public spaces, i.e. roads, sidewalks, open spaces, etc. under the jurisdiction of the municipality.

Based on the previous work described in the Introduction, the selected target population is that most likely to benefit from pavement-watering: pedestrians. The period during which the emergency strategy may be activated spans from the 15<sup>th</sup> of June to the 15<sup>th</sup> of September.

## Case study area: Alésia neighborhood

The neighborhood centered on the Alésia metro station will be considered as a case study area. Figure 2 illustrates its location within Paris intra-muros, respectively outlined with a bold red and black line. In addition, a Google Maps satellite image is provided as well as a map of public parks, urban vegetation and private spaces. This area spans westerly to rue des Plantes, easterly to the RER B train line, northerly to the 14<sup>th</sup> Arrondissement City Hall and southerly to Porte d’Orléans. It comprises a commercial area around the Alésia metro station, mostly surrounded by residential areas and a number of small parks.

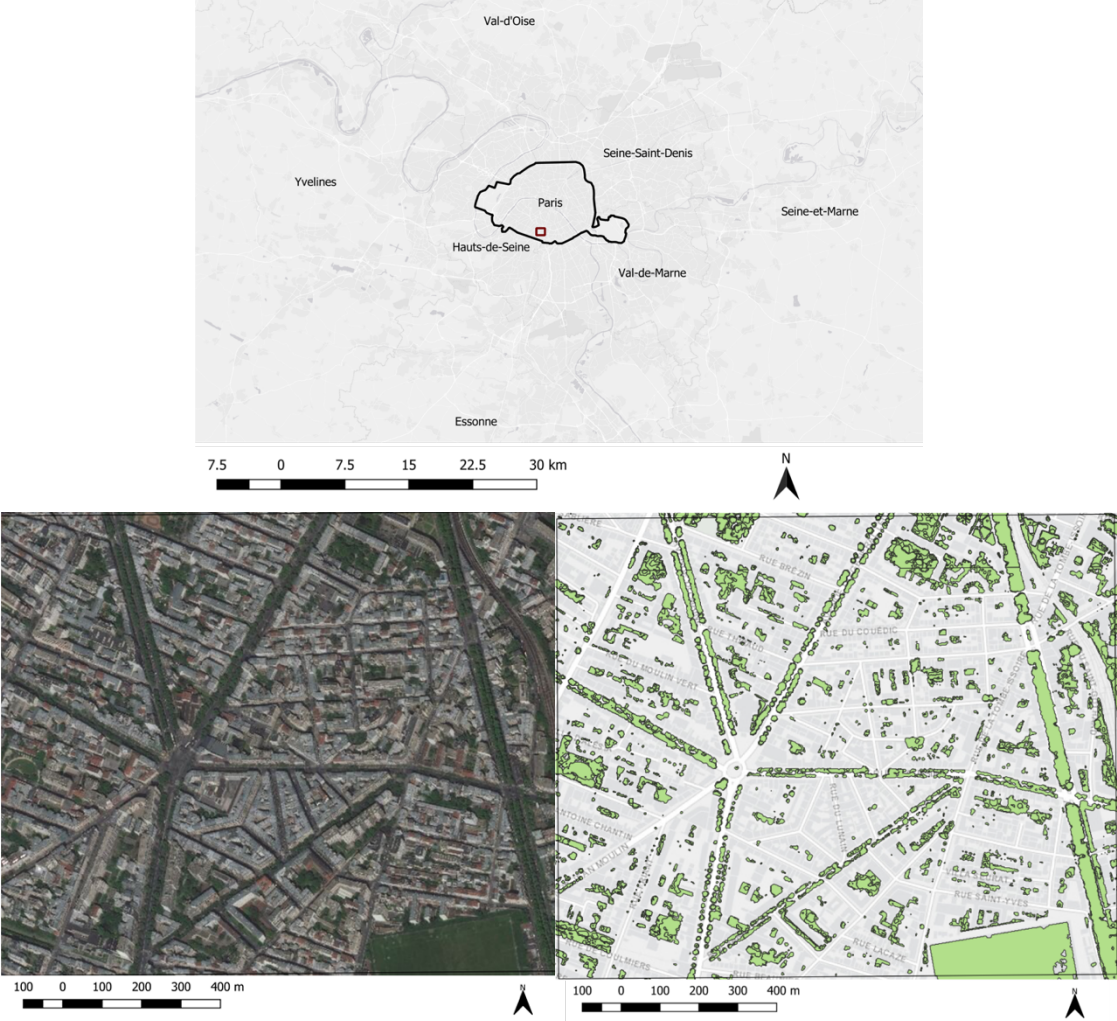


Figure 2: Location of the case area within Paris intra-muros (top), satellite view of case area (bottom left) and vegetative cover (bottom right).

This area will help better illustrate and discuss the different indicators that will be used in this work.

## Dataset Construction and Combination

The aim of the GIS model is to help decision-makers identify high priority areas for pavement-watering in case of a heat wave. Two principal datasets are used for this:

1. Pavement-Watering Cooling Potential
2. Heat-related Health Risk

The analysis of Pavement-watering Cooling Potential is used to identify areas where conditions are met for pavement-watering to be most effective. The Heat-related Health Risk analysis aims to identify areas where the risks associated with heat waves are greatest. Areas combining both indicators will be suggested for pavement-watering in the event of a heat-wave. This requires that the datasets be combined by intersection, i.e. only areas presenting both high heat risk and high cooling potential remain at the end of the process. All the sub-datasets used in their construction are also combined by intersection. Figure 3 summarizes the adopted methodology for dataset construction, indicating what each dataset is built on. The lowest level of the diagram indicates the source databases.

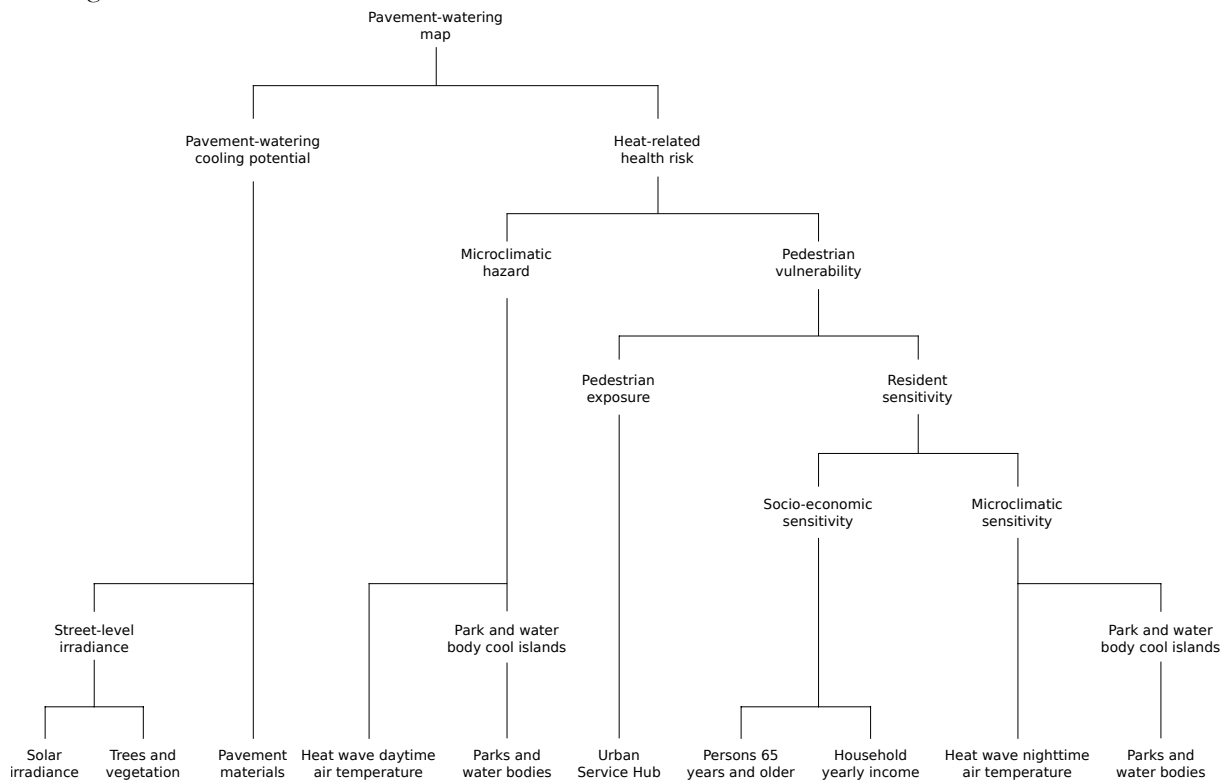


Figure 3: Dataset construction diagram

A preliminary dataset, not shown in Figure 3, is used to delimit the space in which the other datasets are considered: the Target Urban Areas, i.e. public spaces.

The construction method for these datasets and the obtained results are described simultaneously hereafter. Most of the georeferenced datasets were acquired from the open access platforms of the Paris Urbanism Agency (APUR), Paris City Hall and the National Census Bureau INSEE, using the Lambert 93 (RGF 93) reference coordinate system.

## Preliminary Dataset: Target Urban Areas

The target urban areas consist of all impervious public spaces. These spaces are isolated by masking i) private spaces (obtained from cadastral data), ii) public green spaces and iii) water bodies. The resulting target areas are highlighted in orange in Figure 4.

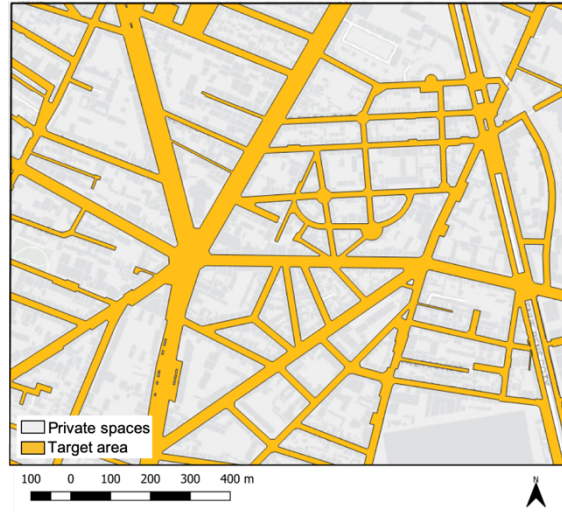


Figure 4: Target areas

## Pavement-Watering Cooling Potential

This spatial indicator represents the potential performance of pavement-watering. As such, the conditions most suited to obtaining effective cooling will be sought out for the case area. On the basis of experimental work conducted to date by the authors [10], two principal factors come into play: solar irradiance and pavement materials.

### Solar Irradiance

Solar irradiance of the targeted pavement surfaces is a crucial parameter in determining the cooling potential of pavement-watering. The period during which watering may be activated spans from June 15<sup>th</sup> to September 15<sup>th</sup>. During this period, which essentially extends from the summer solstice to the autumn equinox, significant variations in horizontal solar irradiance will occur and must be taken into account. To this aim, the global horizontal solar irradiance under clear sky conditions is calculated at a 30-minute timestep. Horizontal extraterrestrial irradiance  $I_{G,ETR}$  and airmass  $AM$  are obtained from the U.S. Department of Energy/NREL/ALLIANCE’s SOLPOS Calculator [30] and are used to calculate global horizontal irradiance  $I_G$  with the following equation [31]:

$$I_G = 1.1 \cdot I_{G,ETR} \cdot 0.7AM^{0.678}$$

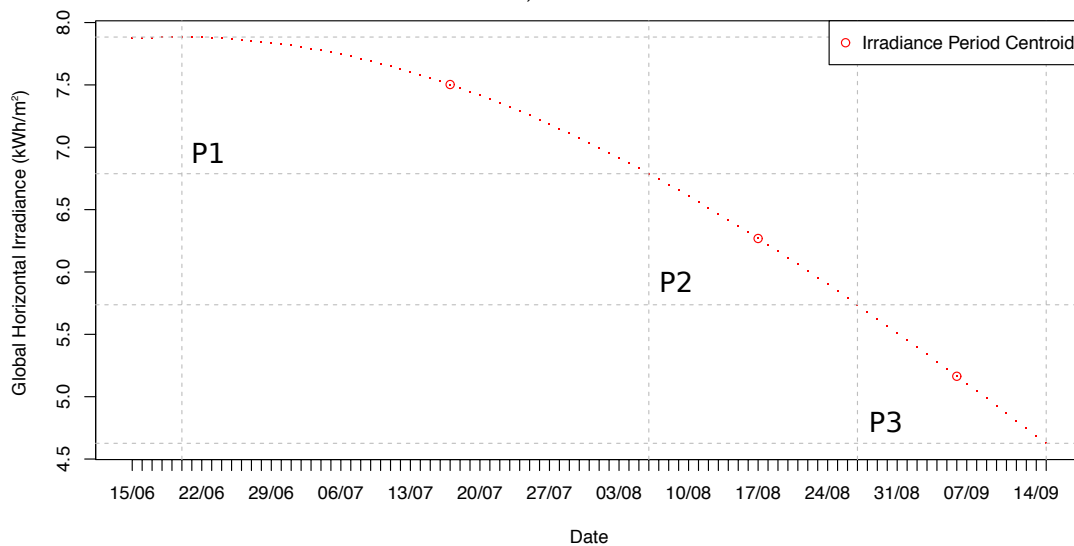


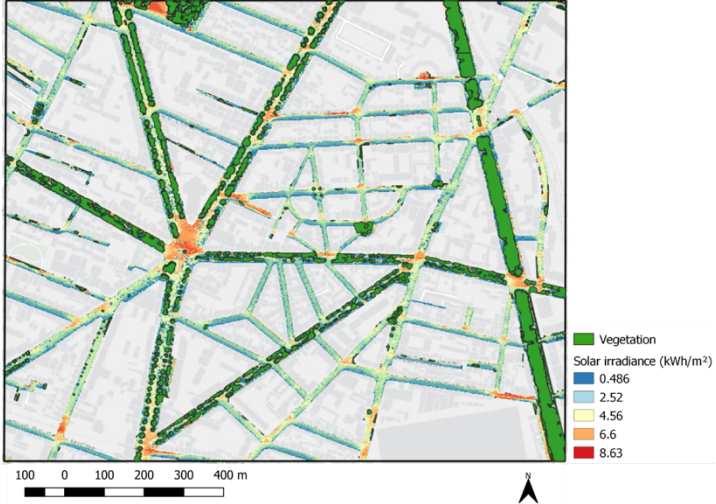
Figure 5: Daily Global Horizontal Irradiance from June 15<sup>th</sup> to September 15<sup>th</sup>.

Figure 5 illustrates the obtained values of daily global horizontal irradiance from June 15<sup>th</sup> to September 15<sup>th</sup>, 2017 in Paris. As previously mentioned, daily irradiance spans a wide range, from 7,88 kWh/m<sup>2</sup> on June 20<sup>th</sup> to 4,63 kWh/m<sup>2</sup> on September 15<sup>th</sup>. The irradiance range is divided into three ranges and the

corresponding timespans categorized into three Irradiance Periods: P1 from June 20<sup>th</sup> to August 6<sup>th</sup>, P2 from August 6<sup>th</sup> to 27<sup>th</sup> and P3 from August 27<sup>th</sup> to September 15<sup>th</sup>. Since June 20<sup>th</sup> is the summer solstice, irradiance values from June 15<sup>th</sup> to 19<sup>th</sup> are identical to irradiance values from June 25<sup>th</sup> to 21<sup>st</sup>, respectively. A single date, called an Irradiance Period Centroid, is chosen to be representative of the solar irradiance pattern for each period. The date is selected such that its daily global horizontal irradiance is approximately equal to the mean irradiance value observed over the considered Irradiance Period. The dates of the three centroids are as follows: July 17<sup>th</sup> for P1, August 17<sup>th</sup> for P2 and September 6<sup>th</sup> for P3.

On these three dates, solar irradiance is simulated for clear sky conditions over Paris based on a 0.5-m resolution digital elevation model (DEM) of Paris constructed from airborne LIDAR measurements dating from 2012. These irradiance simulations are conducted with a 30-minute timestep by APUR using SAGA’s Potential Solar Irradiance tool. A vegetation canopy model, obtained from APUR’s Open Data Platform, is used to filter out vegetation crowns taller than 1 m from this analysis since they are not located at ground level and appear as solid objects in the DEM. This approach could be refined further if data was available on the 3D geometry of the vegetation canopy, e.g. crown upper and lower vertical boundaries, etc.

Two intraday periods are considered, corresponding to the work shifts during which pavement-watering would be conducted: morning (6 am to 12 pm UT) and afternoon (12 pm to 6 pm UT). For the purpose of this paper however, we will only consider daytime (6 am to 6 pm). Figure 6 illustrates the solar irradiance over the case study area simulated on August 17<sup>th</sup>. Its in-field reliability will naturally depend on the DEM’s spatial resolution and its age. A new DEM should be made available shortly by Paris City Hall, constructed in 2018.



**Figure 6: Global solar irradiance of public spaces in the case area. Vegetation taller than 1 meter (green) is filtered out.**

On the basis of this irradiance data, a pavement-watering cooling potential indicator is defined based on an irradiance threshold. This limit corresponds to 50% of global horizontal irradiance for an unmasked surface during the considered period, i.e. half of morning or afternoon cumulative irradiance. For August 17<sup>th</sup>, this corresponds to more than 3.13 kWh/m<sup>2</sup> and is illustrated in Figure 7.

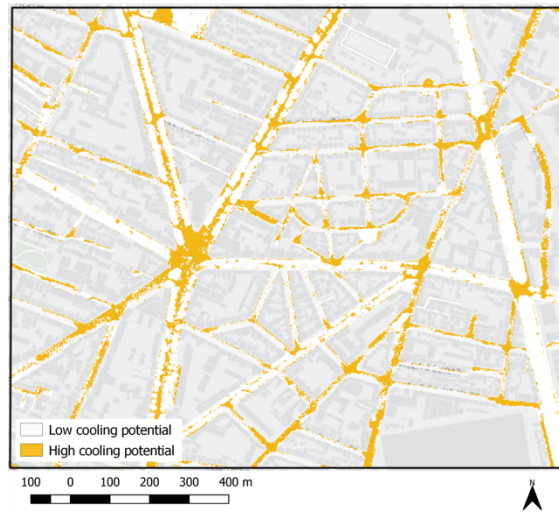


Figure 7: Pavement-watering cooling potential in public spaces in the case area for August 17<sup>th</sup>.

## Pavement Materials

Potential gains from pavement-watering also depend on the materials being watered. Indeed, expected gains are clearly greater for low-albedo surfaces than for those with high albedo. The other thermal properties of those materials can also have an impact [32], [33].

Unfortunately, this information is very difficult to obtain for many urban areas, including Paris. Nevertheless, when available it can be used to improve the accuracy of the potential cooling indicator. Research on the influence of pavement structure composition on the performance of pavement-watering is currently underway [34].

In the absence of an existing georeferenced dataset for existing paving materials in Paris, one of two possibilities are assumed for this study in terms of paving materials: asphalt concrete. Since parks have been excluded from the Target Area, it is unlikely for vegetated surfaces to be present. However, this assumption does neglect the use of granite pavers, stabilized sand, cobblestones or other paving materials which do exist in Parisian public spaces although they are not dominant city-wide.

This assumption results in attributing high cooling potential to all non-vegetated areas of public spaces with solar irradiance exceeding the previously-defined threshold.

In the future, finer knowledge of existing paving materials and better knowledge of the impact of watering a variety of standard Parisian pavement materials will help refine the cooling potential indicator from a threshold to a scale evaluation. The former can be obtained for example from supervised classification in GIS of high resolution photographs, while the latter is the focus of ongoing work by the authors [20], [21].

## Heat-related Health Risk

The daytime heat-related health risk indicator is constructed from three other indicators: microclimatic hazard, population exposure and population vulnerability. They are combined by intersection as follows :

$$\text{Risk} = \text{Hazard} \times \text{Vulnerability} = \text{Hazard} \times (\text{Exposure} + \text{Sensitivity})$$

Microclimatic hazard is taken here as an indicator for pedestrian heat stress under conditions representative of a heat-wave in Paris. Using Turner et al's framework [35], heat-waves are seen here as a perturbation of normal summertime weather conditions.

Vulnerability is defined here on the basis of exposure and sensitivity, without factoring in adaptive capacity as per Cutter et al. [36]. The former is defined as contact between the population and outdoor heat-wave conditions in public places, i.e. a measure of pedestrian traffic. The latter is analyzed here using both socio-economic and microclimatic indicators, seen here as aggravating factors that make a given population more sensitive to damage, e.g. a health event, from exposure to heat-waves during daytime.

No adaptive capacity terms are factored into this analysis. On the one hand, France and Europe exhibit low air conditioning penetration. Furthermore, following the 2003 heat-wave, a number of policies were put in place at the national level to address the related health risk, but these measures are applied nationwide. Therefore, at the spatial scale considered, no differences in adaptive capacity are considered within Paris.

We now describe the methodology used to construct each of these sub-indicators.

## Microclimatic Hazard

The relevant stressor for microclimatic hazard is outdoor heat stress. Air temperature and mean radiant temperature are among the most critical indicators for pedestrian heat stress. Paris is fortunate to have been thoroughly studied from a microclimatic perspective. In particular, the 2003 heat-wave has focused much attention. Taking advantage of this situation, the microclimatic hazard dataset used here is based on existing 2-m air temperature simulations conducted for Paris during the 2003 heat-wave. In addition, the cooling influence of parks and water bodies is emphasized.

### Air Temperature during a heat-wave

Average daytime air temperature at a height of 2 m is obtained from urban canopy simulations of the 2003 heatwave conducted by Météo-France in the framework of the EPICEA Project [13]. The spatial resolution of these simulations is 250 m and the considered heatwave period spans from August 8<sup>th</sup> to 13<sup>th</sup>, 2003, i.e. the warmest period of the heat-wave in France.

To determine the microclimatic hazard, average daytime temperatures, calculated from 6 am to 6 pm are considered.

### Park and Water-Body Cool Islands

The previous dataset includes the cooling influence of parks and water bodies comparable or greater in size to the grid-mesh. However, for those which are smaller than the grid size, the cooling influence is averaged out by their surroundings. To compensate for this effect, the cooling effect of parks and water bodies is emphasized both within and around their boundaries.

Bowler et al. provide a thorough review of the literature pertaining to the cooling influence of parks and water bodies [37]. Unfortunately, it is clear from their work that there is no simple way of determining a park's or water body's cooling impact or area of influence on its surroundings, although the latter is often cited as being on the order of the park's size and characteristic length. On average, a cooling influence of  $\Delta T_{park} = 0.94^\circ\text{C}$  is reported. Often, the park's cooling influence is reported to extend outside its boundary by the park's characteristic length.

Generally-speaking, heat (and mass) transport are described by convection-diffusion equations having the following general form, with  $h$  the air's specific enthalpy,  $u$  the velocity field,  $D$  thermal diffusivity and  $S$  a possible source term:

$$\frac{\partial h}{\partial t} + u\nabla h = D\Delta h + S$$

Under steady-state conditions and since we are interested in heat-wave conditions, which generally offer low wind speeds, convection is neglected reducing the transport equation to Laplace's equation  $\Delta h = 0$  in the absence of a heat source.

For  $h = \rho c_p T$ , with constant  $c_p$ , the equation in spherical coordinates at a given distance  $r$  from the center of the park is:

$$\Delta h = \rho c_p \left[ \frac{1}{r^2} \frac{\partial}{\partial r} \left( r^2 \frac{\partial T}{\partial r} \right) + \frac{1}{r^2 \sin \theta} \frac{\partial}{\partial \theta} \left( \sin \theta \frac{\partial T}{\partial \theta} \right) + \frac{1}{r^2 \sin^2 \theta} \frac{\partial^2 T}{\partial \varphi^2} \right] = 0$$

If, as is illustrated in Figure 8, we consider that the volume of cooled air above a disk-shaped park or water body is spherical in shape of radius  $R$  and at a constant temperature  $T_a - \Delta T_{park}$ , with  $T_a$  the air temperature surround the park, the distribution of temperature  $T(r)$  must satisfy:

$$\frac{1}{r^2} \frac{\partial}{\partial r} \left( r^2 \frac{\partial T}{\partial r} \right) = 0$$

The theoretical boundary conditions are

$$\begin{cases} T_a - T(r = R) = \Delta T_{park} \\ \lim_{r \rightarrow \infty} T_a - T(r) = 0 \end{cases}$$

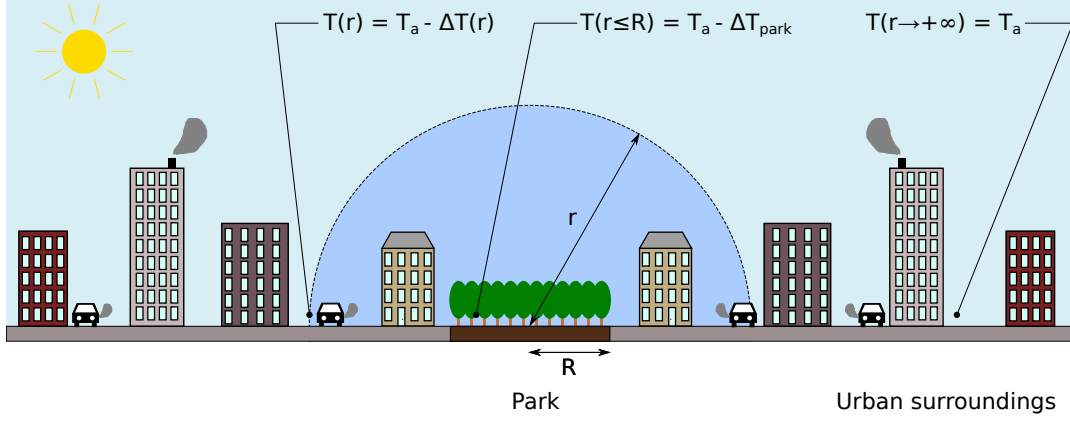


Figure 8: Illustration of a park's cooling influence under no-wind conditions

The analytical solution to this differential equation is:

$$T_a - T(r) = \begin{cases} \Delta T_{park} & \text{for } r < R \\ \Delta T_{park} \frac{R}{r} & \text{for } r \geq R \end{cases}$$

With this model, a fixed temperature reduction of  $\Delta T_{park}$  is considered inside the park or water body, while outside the body the radial temperature reduction decreases asymptotically to zero as the distance  $r$  from the park or water body increases, following an inverse law.

Similar approaches have been used by other authors and the proposed model is consistent with field measurements found in the literature [38]–[40]. The model proposed here however is physically-grounded, based on the assumption that the cooling effect outside the park or water body is driven by thermal diffusion, valid for parks or water bodies. This simplified approach can easily be replaced if a more reliable model of park and water body cool islands becomes available in the future.

Unfortunately, for implementation in GIS, the analytical solution is impractical as an infinite distance cannot be calculated or modelled. We therefore consider the following boundary conditions instead, which assume that the cooling effect decreases to 10% of the intra-park value at a distance  $R$  from the boundary, and is zero thereafter:

$$\begin{cases} T_a - T(r = R) = \Delta T_{park} \\ T_a - T(r = 2R) = \Delta T_{park} / 10 \\ T_a - T(r \geq 2R) = 0 \end{cases}$$

We obtain the following solution:

$$T_a - T(r) = \begin{cases} \Delta T_{park} & \text{for } r < R \\ \Delta T_{park} \frac{18R - 8r}{10r} & \text{for } R \leq r \leq 2R \\ 0 & \text{for } r > 2R \end{cases}$$

For a generically-shaped park or water body, the radius used previously is replaced with the body's characteristic length as determined by approximating its morphology with the minimum bounding rectangle (MBR) calculated with GIS. The MBR is fitted to each body, providing an estimate of its short- and long-axis ( $SA$  and  $LA$ , respectively). A correction is included to account for non-convex parks and water-bodies, i.e. voids within the MBR. The body's characteristic length is defined as half of its short-axis ( $SA/2$ ). Practically-speaking the area of influence of park and water bodies is considered to extend up to a distance of  $SA/2$  outside its boundary.

By replacing the distance  $r$  from the center of body with the distance  $d$  from the boundary, the following equation is obtained and implemented into the GIS:

$$T_a - T(d) = \begin{cases} \Delta T_{park} \left( \frac{10 SA/2 - 8d}{10d + 10 SA/2} \right) & \text{for } 0 \leq d \leq SA/2 \\ 0 & \text{for } d > SA/2 \end{cases}$$

Figure 9 illustrates the resulting park and water body cool islands.

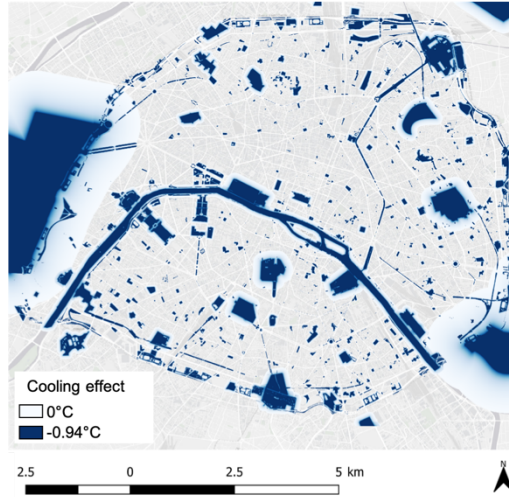


Figure 9: Cooling influence of parks and water bodies

### Microclimatic hazard

The microclimatic hazard is then obtained by adding the cooling effect calculated with this model of park and water bodies to the previously-described EPICEA air temperature simulations. High hazard areas are those with resulting temperatures exceeding a certain threshold.

The heat-wave threshold values for  $BMI_{Min}$  and  $BMI_{Max}$  are respectively  $21^{\circ}C$  and  $31^{\circ}C$  for Paris. These values might be considered a natural first choice, since they are based on epidemiological studies of heat risk. However, given that the simulation data corresponds to an exceptionally warm and long heat-wave and that the case area is the center of the Paris metropolitan area, these heat-wave threshold values are exceeded for almost all grid points, both day and night. These threshold values are therefore poorly selective when using 2003 heat-wave data.

Several options are available to decision-makers at this stage to define relevant values. One approach is to consider the temperature dataset distribution and define a threshold at a given quantile. For example, the first (Q1), second (i.e. the median) Q2, or third (Q3) quartiles can be used to respectively target only the hottest 75%, 50% or 25% of grid points in the case area.

It should be noted however that there is only a  $0.6^{\circ}C$  difference between Q1 ( $35.7^{\circ}C$ ) and Q3 ( $36.3^{\circ}C$ ), of which the health-relevance remains to be demonstrated. In any case, we recommend providing a range of possible thresholds to decision-makers such that the decision remains theirs to make. Figure 10 illustrates areas with high microclimatic hazard with the median value (Q2) chosen as the threshold level.

Future work will see this criterion replaced with more relevant heat stress indicators such as UTCI as modelled outdoors by urban canopy models.

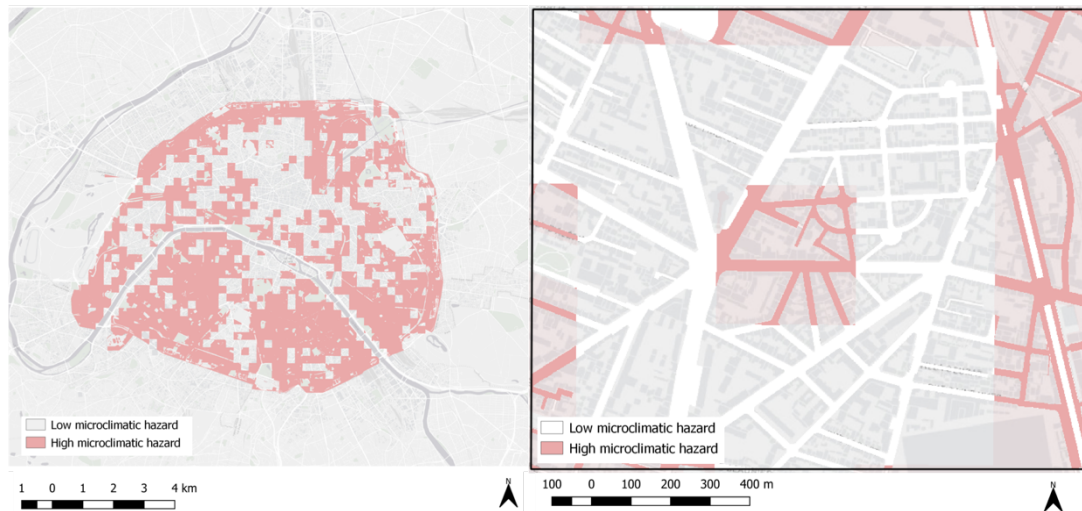


Figure 10: Daytime microclimatic hazard areas (in pink) for Paris intra-muros (left) and the case area (right).

## Pedestrian Vulnerability

The vulnerability of pedestrians to extreme heat is examined here as the combination of their exposure and their sensitivity, as detailed below.

### Pedestrian Exposure

Pedestrian exposure is modelled on the basis of pedestrian traffic. Relevant data can be difficult to obtain, but proxies may be available, e.g. such as has been constructed from the Flickr database [41]. Luckily for Paris, APUR has created and frequently updates a dataset which includes information on pedestrian traffic “Centralité”, which may be loosely translated to “Urban Service Hubs” (USH). This indicator is similar to the Walk Score [42].

This indicator represents the attractiveness of an area by accounting for the presence of urban amenities such as shops, public transportation and public services to identify and categorize public spaces into Local, Mixed or Global scale USH. Local hubs only attract residents from the immediate surroundings while global ones will attract people from across the metropolitan area or even beyond for the highly touristic ones. Mixed hubs have intermediate attractiveness.

USH is used here as an indicator of pedestrian traffic. Any of the three USH scales or combination thereof could be chosen as a threshold for pedestrian exposure. Here, the threshold is set such that any level of USH is considered as high pedestrian exposure.

In addition to USH being used to identify high exposure areas, their scale attribute (local, mixed or global) will also be used to refine the analysis by accounting for where the pedestrians are from. Indeed, while global- and mixed-scale USH have large catchment areas which may span far beyond their immediate surroundings, local-scale USH attract residents from the immediate vicinity only.

As such, local-scale USH vulnerability will be evaluated according to additional information at the local grid mesh scale. In the absence of additional information for global and mixed-scale USH, these areas will be attributed a high level of vulnerability, in light of the intensity of their pedestrian traffic.

Figure 11 illustrates global and mixed-scale USH, modelled as high traffic areas, in pink and local-scale in black, modelled as local traffic, for which more detailed analyses of sensitivity are conducted.

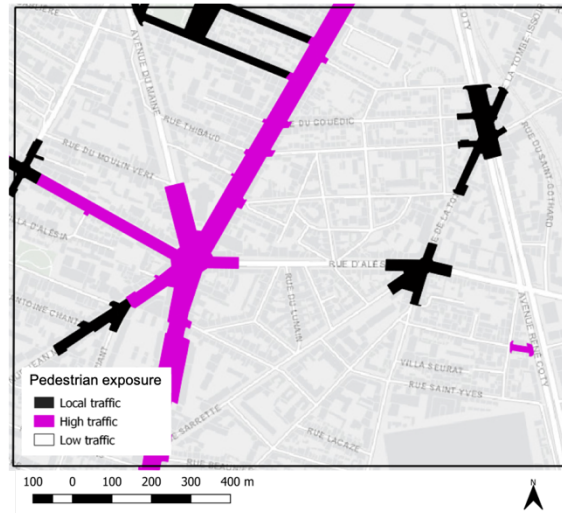


Figure 11: Areas with high pedestrian exposure.

### Resident sensitivity

Two types of information are used for the assessment of resident sensitivity. On the one hand, socio-economic data at the census grid scale, as is typically found in other HVI schemes, will be used to evaluate socio-economic sensitivity. On the other hand, nighttime temperatures will be used to evaluate microclimatic sensitivity.

**Socio-economic sensitivity:** Similarly to other heat vulnerability indices [25]–[28], socio-economic sensitivity is accounted for with socio-economic indicators at the census grid scale of 200 m<sup>2</sup>. Two indicators are used here: the number of persons 65 years old or more and the mean household yearly income. The database is available from the national census bureau (National Institute of Statistics and Economic Studies, INSEE) website<sup>1</sup>. Figure 12 shows the results for the two indicators for Paris, categorized by quintile.

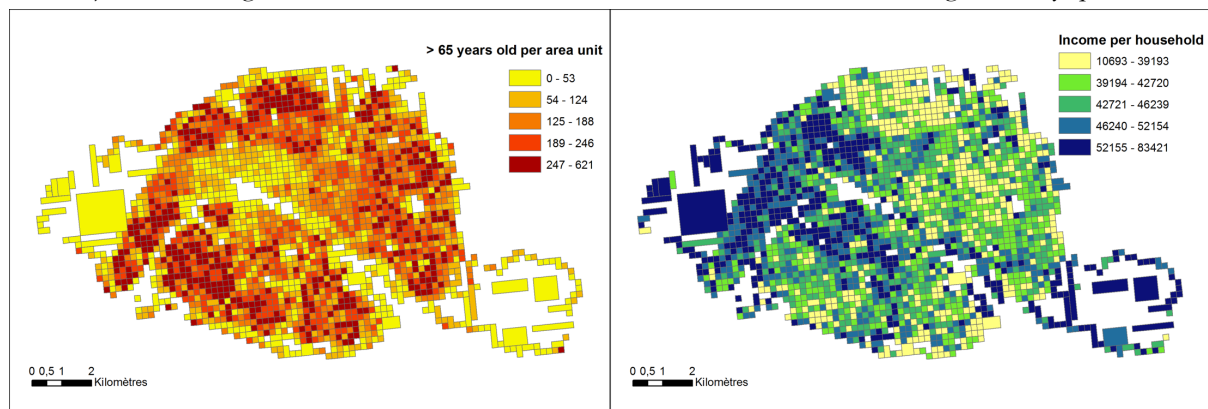


Figure 12: Socio-economic indices at the 200 m<sup>2</sup> unit scale: number of persons aged 65 years or older (left), average yearly income per household in €/year (right).

For the purpose of assessing sensitivity, age sensitivity increases with higher numbers of persons aged 65 years and older, while income sensitivity increases with lower yearly incomes. For this study, a threshold is set at the most penalizing quartile for both indicators: the last quartile for age ( $Q_{age}$ ) and the first quartile for income ( $Q_{income}$ ). On this basis, three levels of socio-economic sensitivity are identified for each grid point: highest quartile of persons 65 years of age and older, lowest quartile of household yearly income or a combination of the two. The resulting socio-economic index is illustrated in Figure 13.

<sup>1</sup> INSEE, 2016. Données carroyées à 200 mètres (200 m gridded data). <https://www.insee.fr/fr/statistiques/2520034>



Figure 13: Socio-economic sensitivity map for Paris (left) and the case area (right).

This socio-economic index can easily be enriched to include other socio-economic data as found fit for the purpose of the heat vulnerability analysis. Future discussions with Public Health France and other heat-related health experts will feed this analysis with indicators relevant to the French socio-economic context and the specifics of its census datasets.

**Microclimatic sensitivity:** The daytime microclimatic hazard dataset defined previously describes the heat stress that pedestrians are exposed to in Parisian public spaces. However, depending on the heat stress that they have experienced at night while they were sleeping at home, they are more or less sensitive to additional daytime heat stress. To address this, an additional microclimatic sensitivity indicator is therefore defined.

To this aim, average nighttime (6 pm to 6 am) temperatures during the 2003 heat-wave are considered, as obtained from the EPICEA Project [13]. Similarly to daytime temperatures, there are several possibilities for defining threshold values, e.g. among nighttime temperature quartiles.

In Figure 14, areas above median (Q50) nighttime temperatures are colored red.

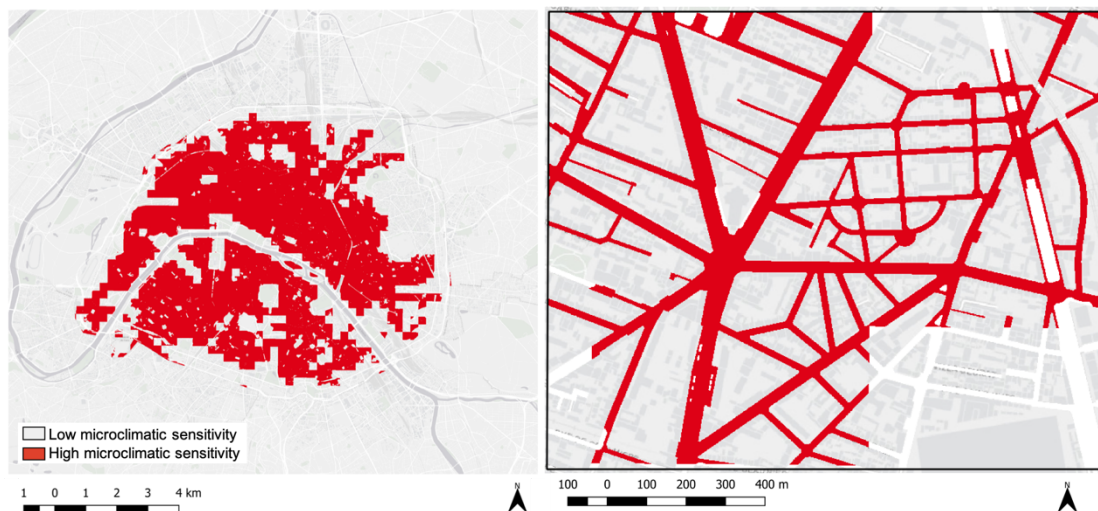


Figure 14: Microclimatic sensitivity map for Paris (left) and the case area (right). Areas with average nighttime air temperatures above the median are highlighted in red.

By merging the sensitivity indicators together, we obtain a multidimensional sensitivity index, illustrated in Figure 15.

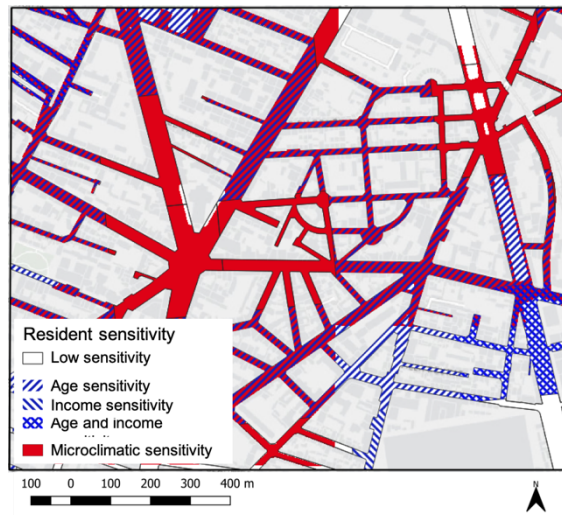


Figure 15: Resident sensitivity.

### Heat Vulnerability

Finally, pedestrian exposure and resident sensitivity are combined to form a single multidimensional vulnerability layer. During this procedure, exposure is used to filter out low pedestrian traffic areas. Furthermore, local traffic areas inherit the resident sensitivity attributes, providing the multidimensional vulnerability illustrated in Figure 16.

At this stage, a threshold can be defined to define high vulnerability areas more accurately.

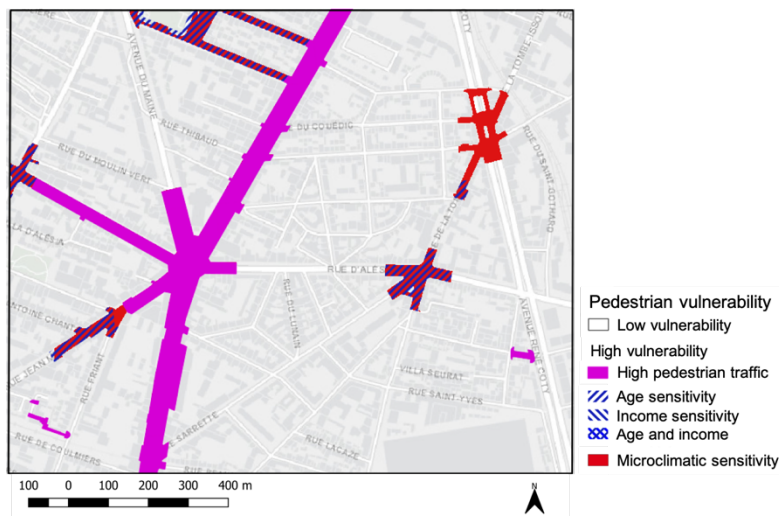


Figure 16: Heat vulnerability map.

### Heat-related Health Risk Map

Figure 17 illustrates the result obtained by intersecting the hazard, exposure and vulnerability indicators to evaluate the overall heat-related health risk. As can be seen, the multidimensionality of the combined heat vulnerability indicator remains, while low hazard and low exposure zones are filtered out.

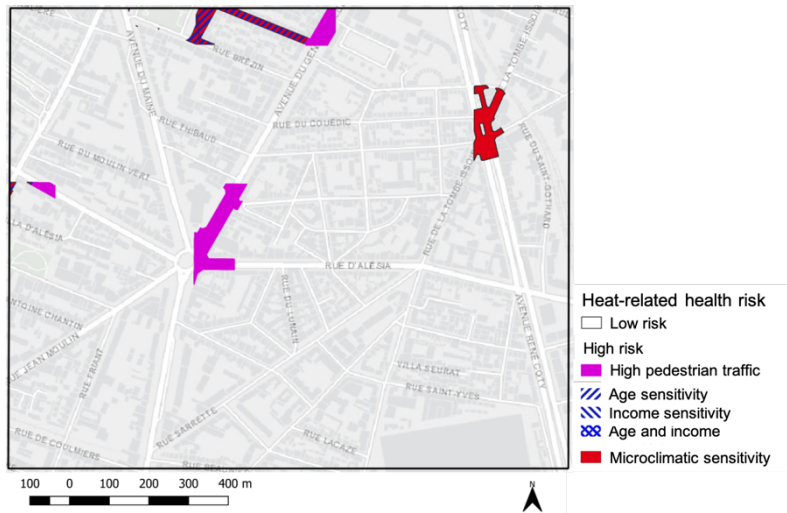


Figure 17: Heat-related health risk map.

As can be seen, the intersection of the previous datasets has filtered out a large portion of the initial case area, mostly due to the presence of many “low” hazard grid points.

## Results and Discussion

Figure 18 presents the resulting map obtained by masking the previous heat-related health risk layer with low pavement-watering cooling potential areas. This only leaves high pavement-water cooling potential areas visible, their heat-related health risk remaining available to define priority levels.

In comparison with Figure 17, the pavement-watering potential dataset has filtered out several pixels due to the presence of trees and highly shaded areas, namely the southern portion of the East-West streets found in the North of the case area.

Overall, urban decision-makers retain a high level of latitude for setting their own thresholds for the different datasets at levels that suit their goals and cities best. Indeed, unless a sound scientific case can be made for selecting a given threshold value for a certain indicator, thresholds should be defined by decision-makers rather than researchers.

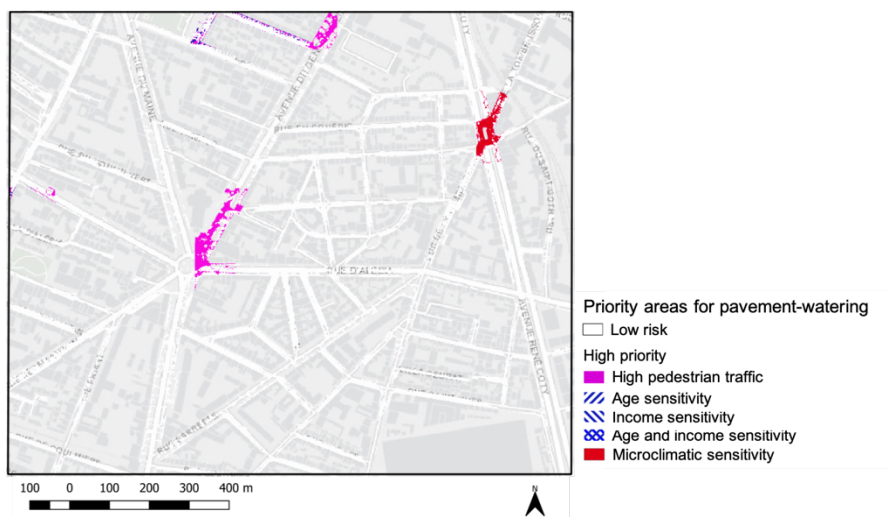


Figure 18: Resulting pavement-watering map.

Among the indicators used here, only for pavement-watering cooling potential can a scientific case be made to select the threshold value which holds a certain physical significance (50% of the period’s cumulative global horizontal irradiance). For the heat risk subsets on the other hand, threshold values are variable and leave room for interpretation and choices by decision-makers which take the local context into account: microclimatic hazard (threshold: median daytime temperatures), pedestrian exposure (threshold: USH areas)

and sensitivity (threshold: most penalizing quartiles for the socio-economic indicators + median nighttime temperatures).

From a practical perspective, the total length of high priority streets for pavement-watering can be used to measure the effort this represents for the city. Depending on what periods within the summer are considered and what thresholds are used, this indicator ranges from 50 to 200 km, out of a total of 2,000 km of streets in Paris, i.e. between 2.5% and 10%.

Assuming that these proportions hold true for the road and sidewalk surface area, this corresponds to between 0.625 km<sup>2</sup> and 2.5 km<sup>2</sup>. Pushing this calculation further with water consumption rates for pavement-watering measured in previous field work in Paris, it can be estimated that watering the identified high priority areas would require between 1,400 and 5,800 m<sup>3</sup>/day or between 0.6 and 2.6 L/day per capita for all of Paris.

These figures are to be compared with daily water consumption in Paris, which totals approximately 500,000 m<sup>3</sup>/day for potable water and 250,000 m<sup>3</sup>/day for non-potable water, i.e. between 0.2% and 0.8% of total Parisian water consumption.

A finer estimation of this amount could be obtained from analyzing the daily solar irradiance of the high priority areas. Going forward, technical feasibility criteria associated with the watering method should also be integrated. These could include thresholds which determine whether or not a street or open space is watered when only a fraction of it has been identified by the scheme, as well as the proximity of the Paris non-potable water network. These criteria and other candidates will be discussed in future work with the relevant stakeholders at Paris City Hall.

Additionally, other criteria should be included to account for the deployment of other heat mitigation methods such as drinking fountains, temporary shading or misting devices, etc. in the future.

## Conclusion

A methodological framework for building a GIS tool to help urban decision makers devise a pavement watering strategy in response to heat waves was proposed. The approach is built on a number of geospatial data layers including an evaluation of pavement-watering's cooling potential for a given area, as well as a heat-related health risk assessment. The latter is built from several subsets including: microclimatic hazard, population exposure and resident sensitivity. To better assess the positive impact of parks and water bodies limiting microclimatic hazard, a physical model park and water body cooling was proposed on the basis of thermal diffusion alone and integrated into the present evaluation.

A case study was presented to illustrate the method and datasets. Different threshold values are required for each subset to conduct the overall analysis. In its final stage, the tool retains much of the information present in the source layers without attempting to aggregate or conflate information of different types, microclimatic indicators with socio-economic ones for instance.

The method was able to focus decision-makers attention on high priority areas representing approximately 2.5% to 10% of total Parisian streets length. Watering these areas would require approximately 1,400 to 5,800 m<sup>3</sup>/day of non-potable water, representing between 0.6 and 2.3% of total non-potable water consumption or 0.6 to 2.6 L/day per capita.

The limitations and room for improvement of the tool and present study lie in the quality and reliability of the datasets that were used. As mentioned in the paper, a number of datasets are hard to come by or must be updated frequently to remain relevant in areas that change the fastest. Among others, the exact boundaries and even mere presence of green spaces and public parks was found to vary significantly according to the dataset used, provided by different sources. To test the quality of readily-available datasets, it may be worthwhile to compare them with satellite-derived information when possible, for example to identify major green areas and water bodies via NVDI. For pavement materials present in public places, recent satellite or street-level imagery of streets is frequently available for many cities. With the input of local expert knowledge, automated techniques, such as supervised GIS classification, may be able to provide a reliable dataset for the purposes of conducting analyses as described here.

Overall, the proposed tool retains significant flexibility, allowing users to adapt it to take the local context into account. This is important as the choice of several threshold values should, in our opinion, ultimately fall on decision-makers for indicators relating to public policy or societal choices where no scientifically-indisputable value can be proposed. While this feature means that using the tool requires some training, it

also promotes better user ownership. It is also an important safeguard against the black-box phenomenon whereby users who fail to grasp the inner workings of decision support tools feel they lack control in the process and disregard the tool and its recommendations.

In the present case, the tool has been presented to Parisian decision-makers and discussions are ongoing to help them develop political and social ownership of the tool. They have been provided with the data required to select and test different thresholds with this aim, particularly those pertaining to the evaluation of the heat-related health risk.

Finally, the tool's flexibility also means that the tool can be used by different kinds of users, not only decision-makers. Indeed, in addition to being able to vary thresholds, users can also focus on, add or remove certain datasets. For example, different or additional sensitivity indicators can be included as deemed necessary for the purposes of public health analyses, while urban planners may only focus on the cooling potential indicator to evaluate the need or relevance of cooling techniques in a space where renovations are being planned independently of the need to adapt the city to climate change.

Future work will seek to build and improve on the presented methodological framework as described here. Further discussions with city stakeholders will help refine the GIS tool to a useable format, while the chosen criteria will continue to be improved for better relevance and accuracy. Other criteria related to the technical feasibility of pavement-watering and the presence of other urban cooling methods are important aspects that will be explored to help complete the tool. Furthermore, the pavement-watering cooling potential indicator will be expanded and adapted to encompass other urban cooling techniques.

## Acknowledgements

Funding for this research was provided by the Water and Sanitation Department of Paris City Hall. The authors thank Julien Bigorgne from APUR for providing us with Parisian insolation data.

## References

- [1] C. Mora *et al.*, "Global risk of deadly heat," *Nat. Clim. Chang.*, vol. 7, no. 7, pp. 501–506, Jun. 2017.
- [2] J. S. Pal and E. A. B. Eltahir, "Future temperature in southwest Asia projected to exceed a threshold for human adaptability," *Nat. Clim. Chang.*, vol. 6, p. 197, Oct. 2015.
- [3] S. Kang and E. A. B. Eltahir, "North China Plain threatened by deadly heatwaves due to climate change and irrigation," *Nat. Commun.*, vol. 9, no. 1, pp. 1–9, 2018.
- [4] A. Lemonsu, R. Koukoku-Arnaud, J. Desplat, J. L. Salagnac, and V. Masson, "Evolution of the Parisian urban climate under a global changing climate," *Clim. Change*, vol. 116, no. 3–4, pp. 679–692, Jul. 2013.
- [5] M. Bador *et al.*, "Future summer mega-heatwave and record-breaking temperatures in a warmer France climate," *Environ. Res. Lett.*, vol. 12, no. 7, p. 074025, Jul. 2017.
- [6] Paris City Council, "Blue Paper," Paris, France (In French), 2012.
- [7] Paris City Council, *La stratégie d'adaptation de Paris*. 2016.
- [8] T. Kinouchi and M. Kanda, "An Observation on the Climatic Effect of Watering on Paved Roads," *J. Hydrosoci. Hydraul. Eng.*, vol. 15, no. 1, pp. 55–64, 1997.
- [9] H. Yamagata, M. Nasu, M. Yoshizawa, A. Miyamoto, and M. Minamiyama, "Heat island mitigation using water retentive pavement sprinkled with reclaimed wastewater," *Water Sci. Technol. a J. Int. Assoc. Water Pollut. Res.*, vol. 57, no. 5, pp. 763–771, Jan. 2008.
- [10] M. Hendel, "Pavement-watering in Cities for Urban Heat Island Mitigation and Climate Change Adaptation : A Study of its Cooling Effects and Water Consumption in Paris, France," Université Paris-Diderot (Paris 7) Sorbonne Paris Cité, 2015.
- [11] P. Maillard, F. David, M. Dechesne, J.-B. Bailly, and E. Lesueur, "Characterization of the Urban Heat Island and evaluation of a road humidification mitigation solution in the district of La Part-Dieu, Lyon (France)," *Tech. Sci. Méthodes*, no. 6, pp. 23-35 (in French), 2014.
- [12] M. Daniel, A. Lemonsu, and V. Viguié, "Role of watering practices in large-scale urban planning strategies to face the heat-wave risk in future climate," *Urban Clim.*, vol. 23, pp. 287–308, Mar. 2018.
- [13] Météo France and CSTB, "EPICEA Project - Final Report," Paris, France (in French), 2012.
- [14] Japan Water Forum, "Let's Uchimizu," 2015. [Online]. Available: <http://www.uchimizu.jp/language/en/>. [Accessed: 20-May-2015].
- [15] M. Hendel, M. Colombert, Y. Diab, and L. Royon, "Improving a pavement-watering method on the basis of pavement surface temperature measurements," *Urban Clim.*, vol. 10, no. December, pp. 189–200, Dec. 2014.
- [16] M. Hendel and L. Royon, "The effect of pavement-watering on subsurface pavement temperatures," *Urban Clim.*, vol. 14, pp. 650–654, Dec. 2015.
- [17] M. Hendel, M. Colombert, Y. Diab, and L. Royon, "An analysis of pavement heat flux to optimize the water

- efficiency of a pavement-watering method,” *Appl. Therm. Eng.*, vol. 78, pp. 658–669, Mar. 2015.
- [18] M. Hendel, P. Gutierrez, M. Colombert, Y. Diab, and L. Royon, “Measuring the effects of urban heat island mitigation techniques in the field: Application to the case of pavement-watering in Paris,” *Urban Clim.*, vol. 16, pp. 43–58, Jun. 2016.
- [19] S. Parison, M. Hendel, K. Jurski, and L. Royon, “The Impact of Different Watering Strategies on the Cooling Effects of Pavement-Watering during Heat-Waves,” in *PLEA 2017 Proceedings - Design to Thrive*, 2017, pp. 120–127.
- [20] M. Hendel, S. Parison, A. Grados, and L. Royon, “Which pavement structures are best suited to limiting the UHI effect? A laboratory-scale study of Parisian pavement structures,” *Build. Environ.*, vol. 144, pp. 216–229, Oct. 2018.
- [21] S. Parison, M. Hendel, A. Grados, K. Jurski, and L. Royon, “A lab experiment for optimizing the cooling efficiency and the watering rate of pavement-watering,” *Urban Clim.*, vol. 31, p. 100543, Mar. 2020.
- [22] P. K. Tsin, A. Knudby, E. S. Krayenhoff, H. C. Ho, M. Brauer, and S. B. Henderson, “Microscale mobile monitoring of urban air temperature,” *Urban Clim.*, pp. 1–15, 2016.
- [23] H. C. Ho, A. Knudby, Y. Xu, M. Hodul, and M. Aminipouri, “A comparison of urban heat islands mapped using skin temperature, air temperature, and apparent temperature (Humidex), for the greater Vancouver area,” *Sci. Total Environ.*, vol. 544, pp. 929–938, 2016.
- [24] I. Keramitsoglou, C. T. Kiranoudis, G. Ceriola, Q. Weng, and U. Rajasekar, “Identification and analysis of urban surface temperature patterns in Greater Athens, Greece, using MODIS imagery,” *Remote Sens. Environ.*, vol. 115, no. 12, pp. 3080–3090, 2011.
- [25] K. Bradford, L. Abrahams, M. Hegglin, and K. Klima, “A Heat Vulnerability Index and Adaptation Solutions for Pittsburgh, Pennsylvania,” *Environ. Sci. Technol.*, vol. 49, no. 19, pp. 11303–11311, 2015.
- [26] S. G. Nayak *et al.*, “Development of a heat vulnerability index for New York State,” *Public Health*, vol. 161, pp. 127–137, 2018.
- [27] D. P. Johnson, A. Stanforth, V. Lulla, and G. Luber, “Developing an applied extreme heat vulnerability index utilizing socioeconomic and environmental data,” *Appl. Geogr.*, vol. 35, no. 1–2, pp. 23–31, 2012.
- [28] T. Wolf and G. McGregor, “The development of a heat wave vulnerability index for London, United Kingdom,” *Weather Clim. Extrem.*, vol. 1, no. August 2003, pp. 59–68, 2013.
- [29] E. Mallen, B. Stone, and K. Lanza, “A methodological assessment of extreme heat mortality modeling and heat vulnerability mapping in Dallas, Texas,” *Urban Clim.*, vol. 30, p. 100528, Dec. 2019.
- [30] NREL, “National Renewable Energy Laboratory Measurement and Instrumentation Data Center Solar Position and Intensity (SOLPOS) Calculator.” <<http://www.nrel.gov/midc/solpos/solpos.html>>, 2017.
- [31] A. B. Meinel and M. P. Meinel, *Applied Solar Energy*, Addison We. 1976.
- [32] Y. Qin and J. E. Hiller, “Understanding pavement-surface energy balance and its implications on cool pavement development,” *Energy Build.*, vol. 85, pp. 389–399, Dec. 2014.
- [33] D. Yinfei, W. Shengyue, and Z. Jian, “Cooling asphalt pavement by a highly oriented heat conduction structure,” *Energy Build.*, vol. 102, pp. 187–196, Sep. 2015.
- [34] S. Parison, M. Hendel, A. Grados, K. Jurski, and L. Royon, “A lab experiment for optimizing the cooling efficiency and the watering rate of pavement-watering,” in *ICUC10 & 14th Symposium on Urban Environment*, 2018.
- [35] B. L. Turner *et al.*, “A framework for vulnerability analysis in sustainability science,” *Proc. Natl. Acad. Sci. U. S. A.*, vol. 100, no. 14, pp. 8074–8079, 2003.
- [36] S. L. C. ã *et al.*, “A place-based model for understanding community resilience to natural disasters,” vol. 18, pp. 598–606, 2008.
- [37] D. E. Bowler, L. Buyung-Ali, T. M. Knight, and A. S. Pullin, “Urban greening to cool towns and cities: A systematic review of the empirical evidence,” *Landsc. Urban Plan.*, vol. 97, no. 3, pp. 147–155, Sep. 2010.
- [38] K. J. Doick, A. Peace, and T. R. Hutchings, “The role of one large greenspace in mitigating London ’ s nocturnal urban heat island,” *Sci. Total Environ.*, vol. 493, pp. 662–671, 2014.
- [39] W. Lin, T. Yu, X. Chang, W. Wu, and Y. Zhang, “Calculating cooling extents of green parks using remote sensing: Method and test,” *Landsc. Urban Plan.*, vol. 134, pp. 66–75, 2015.
- [40] S. Hamada and T. Ohta, “Seasonal variations in the cooling effect of urban green areas on surrounding urban areas,” *Urban For. Urban Green.*, vol. 9, no. 1, pp. 15–24, 2010.
- [41] A. Swanson, “Fascinating maps show the different places locals and tourists go in 19 major cities,” *Washington Post*, 2016.
- [42] L. J. Carr, S. I. Dunsiger, and B. H. Marcus, “Walk Score™ As a Global Estimate of Neighborhood Walkability,” *AMEPRE*, vol. 39, no. 5, pp. 460–463, 2010.